

Enhanced Boundary Learning for Glass-like Object Segmentation

Hao He^{1,2*}, Xiangtai Li^{3*}, Guangliang Cheng^{4,6}, Jianping Shi^{4,5},
Yunhai Tong³, Gaofeng Meng¹, Véronique Prinet¹, Lubin Weng¹,

¹ NLPR, Institute of Automation, Chinese Academy of Sciences

² School of Artificial Intelligence, University of Chinese Academy of Sciences

³ Key Laboratory of Machine Perception (MOE), Peking University

⁴ SenseTime Research ⁵ Qing Yuan Research Institute, SJTU ⁶ Shanghai AI Laboratory

Abstract

Glass-like objects such as windows, bottles, and mirrors exist widely in the real world. Sensing these objects has many applications, including robot navigation and grasping. However, this task is very challenging due to the arbitrary scenes behind glass-like objects. This paper aims to solve the glass-like object segmentation problem via enhanced boundary learning. In particular, we first propose a novel refined differential module for generating finer boundary cues. Then an edge-aware point-based graph convolution network module is proposed to model the global shape representation along the boundary. Both modules are lightweight and effective, which can be embedded into various segmentation models. Moreover, we use these two modules to design a decoder to get accurate segmentation results, especially on the boundary. Extensive experiments on three recent glass-like object segmentation datasets, including Trans10k, MSD, and GDD, show that our approach establishes new state-of-the-art performances. We also offer the generality and superiority of our approach compared with recent methods on three general segmentation datasets, including Cityscapes, BDD, and COCO Stuff. Code and models will be available at (<https://github.com/hehao13/EBLNet>).

1. Introduction

Glass-like objects widely exist in the real world: bottles, windows, and mirrors are made of glass. They are mostly transparent, often amorphous solid. Sensing these objects is useful for many applications. For example, robots need to avoid fragile objects (i.e., glasses, vases, bowls, and mirrors) during their navigation. These objects differ from others in that: (i) they do not have a fixed pattern, their

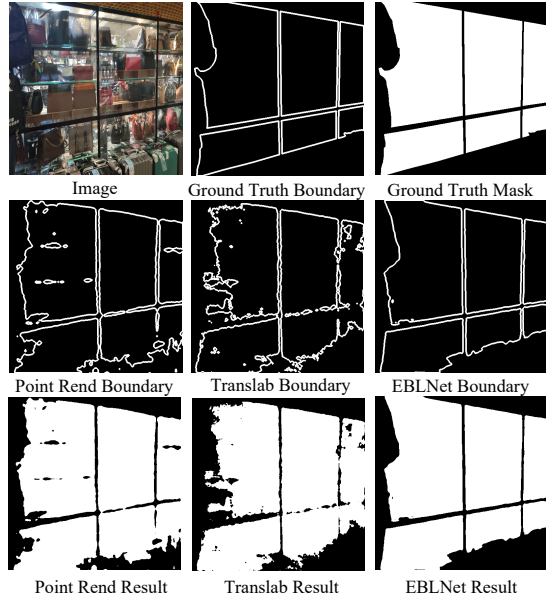


Figure 1: Illustration of glass-like object segmentation. Row one gives the input image and ground truth. Row two shows the comparison results on the boundary. Row three compares the final segmentation results. Our method (EBLNet) works the best among them [30, 61].

shape often vary; (ii) because of their transparent nature, they are mostly confounded with the surrounding background, the appearance of their inner region varying according to the scene; (iii) not all glass regions are salient, sometimes there are some occlusions or reflections on it. These problems make such glass-like object segmentation a difficult task. Current state-of-the-art semantic segmentation models [73, 8, 15, 34] and salient object detection methods [41, 70] are significantly challenged. Similarly, though previous works on boundary detection [63, 69, 13] achieve remarkable results on traditional benchmarks [54, 1], they

*The first two authors contribute equally.

can not work well on glass-like object scenarios due to the confounding appearance of the object’s inner and outer parts. Fig. 1 illustrates a complex example for glass segmentation.

To address the above issues, the first step is to construct large-scale datasets [47, 65, 61]. From these datasets, the task is cast as a two-class semantic segmentation problem, where glass-like objects are foreground and the rest is background. Based on these newly proposed datasets, state-of-the-art methods of both semantic segmentation [15, 73, 8] and salient object detection [41, 60] obtain unsatisfactory results. For example, DeeplabV3+ (semantic segmentation method) [8] and EGNet (salient object detection method) [74] only get 84.2 and 85.0 mIoU on GDD [47] test set. Very few dedicated methods to solve this challenging task have been introduced so far [47, 61, 65]. GDNet [47] proposes to use multiple well-designed large-field contextual feature integration to enhance the context representation for modeling glass object context. MirrorNet [65] uses a contextual contrasted feature extraction module for mirror detection. In contrast, Translab [61] proposes to use boundary-aware information to improve the segmentation performance. However, the first two [65, 47] bring redundancy for context modeling, which needs specific human designs for each task. The last one ignores the pixel-wise relationship on the boundary, limiting the generality of learning objects with various shapes.

When humans locate and recognize the glass-like object, one crucial cue is the entire boundary of such object: comparing the inner object appearance and its surrounding background cannot help much to segment since they are mainly confounded.

To reduce the influence of complex inner parts and get accurate boundary prediction, motivated by differential edge detection and morphological processing [14, 50], we propose a novel and efficient module named Refined Differential Module (RDM). RDM works in a coarse-to-fine manner with residual learning. Specifically, rather than simply predict the edge of objects with edge supervision, we also supervise the non-edge part following the same spirit of dilation operation in morphological processing [52] to eliminate noise brought by the inner part and background. This process helps generate smoother non-edge features. Then the thinner and accurate edge features can be generated by subtracting the non-edge features from the whole features. In order to use the precise edge prediction to enhance global feature learning around the edge and improve the final prediction, we further propose an efficient edge-aware Point-based Graph convolution network Module (PGM). In network design, our modules can be plugged into many semantic segmentation methods. Take DeeplabV3+ [8] as an example, our modules can be inserted behind the ASPP module. Finally, we propose a joint loss function to simul-

taneously supervise the edge part, non-edge part, and final result.

Quantitatively, our approach achieves a significant gain in performance w.r.t. previous work [30, 61] (around 3%-5% in mIoU), on three recent glass-like object segmentation datasets (Trans10k [61], GDD [47], and MSD [65]), and hence achieves a new state-of-the-art. *Visually*, our method detects more accurate boundaries, resulting in a more precise segmentation result (see Fig. 1). This backs our original motivation that finer boundary prediction leads to more refined segmentation.

We further apply our approach on another three general segmentation datasets, including Cityscapes [12], BDD [67], and COCO Stuff [4]. Compared with the recent method [30], our method achieves better results, which indicates the generality and effectiveness of our approach. Our main contributions are three-fold:

- We propose a novel Refined Differential Module (RDM) to generate accurate boundary and an efficient Point-based Graph convolution network Module (PGM) for global edge feature learning. Then a joint loss function is proposed to supervise the whole model.
- Extensive experiments and analysis indicate the effectiveness of our proposed modules. We achieve state-of-the-art results on three challenging recent glass-like object segmentation benchmarks.
- We also verify our method’s generality on three general segmentation datasets, including Cityscapes, BDD, COCO Stuff.

2. Related Work

Semantic Segmentation: Recent methods for semantic segmentation are predominantly based on FCNs [45]. Several works [40, 76, 44, 22] use some structured prediction modules like conditional random fields (dense CRFs) to refine outputs. Current state-of-the-art methods [73, 7, 15, 36] improve the segmentation performance by designing specific heads with dilated convolutions [68] to capture contextual information. Recently, non-local operators [58, 15, 18, 36, 79, 25, 17, 35] based on the self-attention mechanism [56] are used to harvest pixel-wise context from the whole image. Similarly, graph convolution networks [38, 37] propagate information over the entire image by reasoning in the interaction space. Although these methods achieve state-of-the-art results on standard benchmarks such as Cityscape [12], ADE [77], BDD [67], and COCO Stuff [4], their performance on glass-like object segmentation benchmarks will drop a lot due to noise of background context that are introduced by the non-local operators. Our method focuses more on the edges and avoids introducing too much background information.

Salient Object Detection: Glass-like-object can also be viewed as one specific case of salient object detection. Many state-of-the-art deep models [70, 42, 71, 74, 49, 75, 16] are devoted to fully utilize the integration of multi-level features to enhance network performance. Recent works [43, 9] apply attention mechanisms to learn both global and local context or adopt foreground/background attention maps to help detect salient objects and eliminate non-salient objects. Our work also utilizes the multi-scale feature representation by designing a cascade differential refined model for better location cues to get fine-grained masks.

Boundary Processing: Boundary processing is a classical computer vision problem. In the era of deep learning, some CNN-based methods have significantly pushed the development of this field, such as [63, 46, 32, 20, 13, 53]. Several works have been proposed to obtain satisfactory boundary localization with structure modeling, such as boundary neural fields [2], affinity field [28] and random walk [3]. Recently, PointRend [30] is proposed to refine the coarse masks by rendering them through one shared multi-layer perception module. Some works [10, 11, 33] fuse to learned edge map into segmentation head to improve segmentation performance on the boundary, while GSCNN [55] uses a gated layer to control the information flow between edge part and regular part. All these works focus on locally mining the edge information and ignore the global shape information, which is essential for recognizing the glass-like objects. Our PGM uses global edge features to improve the segmentation results of glass-like objects.

Glass-like Object Segmentation: Glass object segmentation comprises two sub-tasks, sometimes processed in a distinct way: mirror segmentation and transparent object segmentation. Mirror segmentation is a new research topic that aims to segment mirror regions from a single RGB image. In [65], the author proposes a large benchmark for this topic. They attempt to use contextual contrasted features in a segmentation scheme. However, contrasted features may not help for transparent object segmentation since semantic and low-level discontinuities in mirrors may not happen for transparent objects. Transparent object segmentation is also a new and challenging task. It aims to segment transparent objects from a single RGB image. In [27], the author uses a polarization camera to capture multi-modal imagery to enhance the transparent object segmentation. Authors of both [47] and [61] propose a new benchmark for this task. [61] proposes TransLab to encode the boundary information while [47] integrates abundant contextual cues. Both of them have failed to explore the relationship between edge features and non-edge features, which are well-considered in our method. The recent work [62] extends previous work [61] into a semantic segmentation task and proposed a transformer based segmentation method [6] to

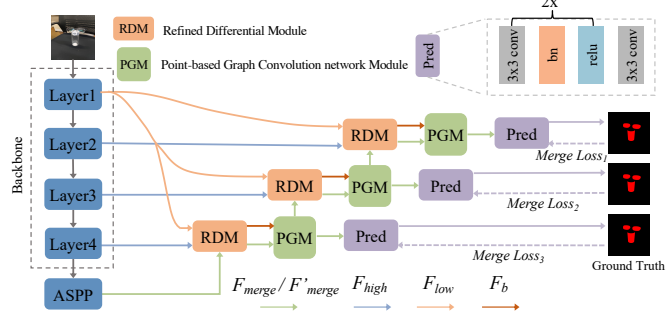


Figure 2: Cascade Network Architecture. We adopt DeeplabV3+ as baseline for illustration where the RDM and PGM are connected in a cascaded order. Best view it on screen and zoom in.

solve it.

3. Method

3.1. Overview

Our framework utilizes and combines the different levels of feature maps (high-level for semantic, low-level for edge-like features) obtained from a pre-trained backbone network. Our observation has two-fold: (i) edge information (from low-level feature maps) are necessary to ‘reinforce’ semantic region cues (obtained from high-level maps); (ii) precise and robust delineation of edges/boundaries enables a fine and accurate segmentation result. This observation leads us to design two modules: (i) A Refined Differential Module (**RDM**) generates (a) the precise and sharpen boundaries of the glass-like objects, (b) the initial segmentation features (Sec. 3.2); (ii) An edge-aware Point-based Graph convolution network Module (**PGM**) learns to refine the final segmentation results using the precise boundary generated by the RDM, it appears in coupling with the RDM (Sec. 3.3). The modules are supervised in three fashions: boundaries-wise, residual-wise (nonboundary-wise), and merge-wise. These two modules are integrated into a cascaded architecture network (Sec. 3.4). Fig. 2 illustrates the overall framework.

3.2. Refined Differential Module

Overview: The structure of RDM is shown in Fig. 3(a), inputs of the RDM are F_{low} , F_{high} and F_{in} , which are low-level features of backbone, relative high-level features of backbone, and outputs of other modules (such as ASPP module in DeeplabV3+ [8]), respectively. Normally, compared with F_{high} , F_{in} has a larger receptive field and is smoother. With these three inputs, RDM aims to learn: (1) precise edge prediction, F_b , (ii) ‘residual’ feature maps, $F_{residual}$ (or features of object inner region at coarse scale), (iii) ‘complete’ segmentation feature maps, F_{merge} , (that characterizes both inner region and boundaries), which

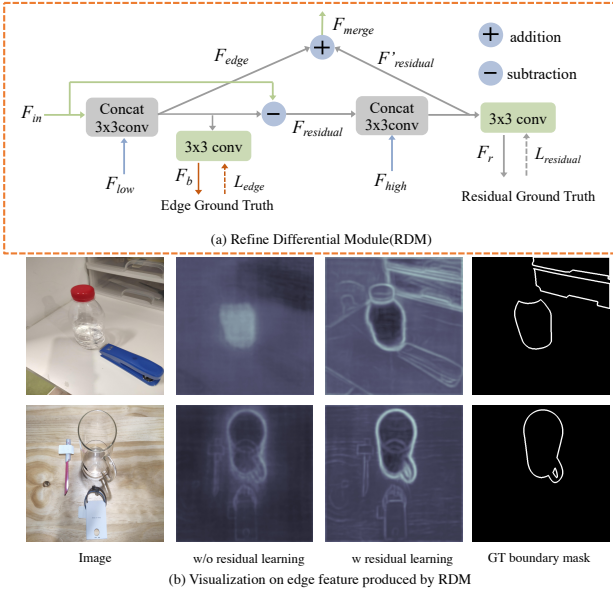


Figure 3: (a) Refined Differential Module, L_{edge} and $L_{residual}$ are losses of edge part prediction and residual part prediction. (b) Feature visualization comparison. The second and the third column represent the edge feature F_{edge} before and after using fine-grained edge prediction with residual learning. After using residual learning, the edge feature F_{edge} is more discriminative. Best view it on screen and zoom in.

serves as the input of the next module. Supervision is applied for each feature type. Since there are two refinements and one subtraction (which will be explained later) of our module, we name it Refined Differential Module or RDM for short.

Coarse edge prediction: This step generates the edge prediction F_b and non-edge features $F_{residual}$. Since low-level features F_{low} can provide detailed positional cues for edge prediction proven in previous works [8, 30], we first **refine** the input feature F_{in} with low-level features F_{low} (after bi-linearly resizing the feature maps) by first concat them. Then, a convolution operator is used to get the refined input feature, $F_{edge} \in \mathbb{R}^{H \times W \times C}$, this process can be formulated by Equ. 1.

$$F_{edge} = g_{3 \times 3}([F_{low}; F_{in}]) \quad (1)$$

where $[;]$ and $g_{n \times n}$ denote concatenation and convolution respectively. Additionally, we compute the residual (*i.e.* non-edge residual-wise) feature $F_{residual}$ by **subtracting** F_{edge} from F_{in} , *i.e.* the difference between the coarse edge map F_{edge} and the input features F_{in} . This procedure can be formulated as Equ. 2:

$$F_{residual} = F_{in} - F_{edge}, \quad (2)$$

We further transform F_{edge} to the edge prediction $F_b \in$

$\mathbb{R}^{H \times W \times 1}$ (via a 2-layer convolution), that will be supervised using a ground-truth edge map.

Fine-grained Edge Prediction with Residual Learning:

Our motivation has two-fold: (1) For the glass-like objects, the inner part may bring noises for edge prediction. Better feature representation of the residual part will make it easier to learn a better edge around the glass-object. (2) Since edge-aware feature F_{edge} generated from the first step may not be very accurate, the subtraction operation may remove some vital features for $F_{residual}$. So we adopt another fine-grained feature F_{high} generated from the backbone to **refine** $F_{residual}$ and get $F'_residual$ for better residual learning. This process is formulated by Equ. 3.

$$F'_residual = g_{3 \times 3}([F_{residual}; F_{high}]) \quad (3)$$

The prediction F_r of the residual part is generated using another two 3×3 convolution layers, which is shown in Equ. 4

$$F_r = g_{3 \times 3}(F'_residual) \quad (4)$$

F_r will be supervised using a ground truth residual mask. This indirect supervision of $F'_residual$ forces it to be smooth, without spurious noise. The convolution operation here performs a similar role as a dilation in morphological processing [50] (*i.e.* making inner part ‘grow up’ towards borders). Finally, we have F_{merge} using Equ. 5 :

$$F_{merge} = F'_residual + F_{edge} \quad (5)$$

F_{merge} is then used to generate the prediction F_m using a segmentation head consisting of three convolutional layers, two batch normalization layers [26], and two non-linear activation function, shown in Fig. 2 (the purple module: Pred).

To best show the effect of our module, we give the feature visualization on F_{edge} for both coarse edge prediction and fine-grained edge prediction with residual learning in Fig. 3(b). We use Principal component analysis (PCA) [59] to reduce the dimension of F_{edge} into three dimensions for visualization. Compared to only supervising the edge part, joint supervision on both edge and residual part can produce more accurate edge features, which supports our motivation for edge sharpening via residual learning.

3.3. Edge-aware Point-based GCN Module

In order to enforce finer boundary delineation on F_{merge} , we further propose an efficient Point-based Graph convolution network Module (GCN). The key idea is to exploit the accurate edge prediction F_b to update the feature map of F_{merge} at the boundary points. To do so, our module accounts for the spatial correlation between edge points. We coin this module Point-based GCN Module (PGM).

Recall on Graph Convolution Network: Graph convolution [29] is a highly efficient and differentiable module that allows long-range interaction in a single operation. Given a

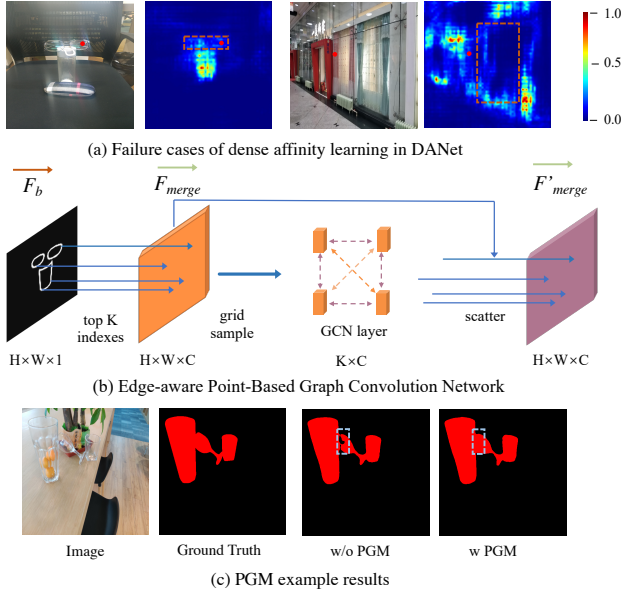


Figure 4: Proposed Point-based Graph convolution Module (PGM). (a) shows two failure cases for dense affinity learning in DANet [15], selected points are marked red. For the first and the second images, the red point is on the glass, while its affinity map mainly comes from the bottle not the glass. For the third and the fourth images, the affinity map of the red point does not come from the glass to which it belongs. (b) describes the pipeline of PGM. (c) proves the effectiveness of PGM. After using PGM, the boundary is much smoother and more consistent. Best view it on screen and zoom in.

graph $\mathbb{G} = \{\mathbb{E}, \mathbb{V}\}$ where \mathbb{V} the nodes and \mathbb{E} the pairwise links between nodes, the graph convolution operation can be defined as [29] with Equ. 6 :

$$\tilde{\mathbf{X}} = \sigma(\mathbf{W} \mathbf{X} \mathbf{A}) \quad (6)$$

with $\sigma(\cdot)$ a non-linear activation function, $\mathbf{A} \in \mathbb{R}^{N \times N}$ is the adjacency matrix characterising the neighbourhood relations of the graph, $\mathbf{W} \in \mathbb{R}^{D \times \tilde{D}}$ is a weight matrix and \mathbf{X} is a $D \times N$ matrices characterizing the N nodes in a D dimensional space. However, directly applying GCN as dense affinity graph [15, 36] for glass-like object segmentation task is a trivial solution since the huge appearance gap on the surface of glass objects. As shown in Fig. 4(a), with the dense affinity graph, inner parts can not provide the context cues to support the final prediction on the visualized affinity maps. Thus we apply GCN only on point-wised boundary features of F_{merge} to enhance its representation.

Point-based Graph Convolution Network on edge: The pipeline of PGM is shown in Fig. 4(b). Given edge prediction F_b and segmentation feature F_{merge} , we sample the nodes V from F_b according to their confidence score and give them attributes from F_{merge} . Specifically, we first select at most K points with the highest confidence in F_b . Then, we use the indices of these points to sample the cor-

responding K point features from F_{merge} . This allows us to build the feature matrix $\mathbf{G}_{in} \in \mathbb{R}^{C \times K}$, where C is the channel dimension of the feature maps in F_{merge} . Assuming a fully connected graph (all K points are connected), the graph convolution operation can be performed as a fully connected layer. Then the adjacency matrix \mathbf{A}_g is simply a 1×1 convolutional layer that is learned in a standard back-propagated way. Then we can write the output features with Equ. 7 :

$$\mathbf{G}_{out} = \sigma(\mathbf{W}_g \mathbf{G}_{in} \mathbf{A}_g) \quad (7)$$

with $\mathbf{A}_g \in \mathbb{R}^{K \times K}$. $\mathbf{W}_g \in \mathbb{R}^{C \times C}$ is a feature projection matrix, that is learned along with \mathbf{A} . After applying one layer of graph convolution and obtaining \mathbf{G}_{out} , we place back the point features of \mathbf{G}_{out} into F_{merge} according to their indices.

PGM is efficient and effective in handling glass-like transparent objects since the global edge information is essential to recognize a glass-like object. As shown in Fig. 4(c), after PGM, the final segmentation boundary is smoother and more consistent.

3.4. Network Architecture and Loss function

In this section, we will give a detailed description of network architecture and loss function design.

Cascade Refined Decoder: Cascade refinement has been proven effective for various tasks [5, 39]. We design a cascade decoder, for each stage, we take the output of PGM F'_{merge} as the new input F_{in} for the next stage RDM while the F_{high} is designed by introducing different stages' features of the backbone network. As the low-level features are essential for detecting object boundaries, we add F_{low} as input for every stage's RDM. We use the F_m of the last cascade layer as the final output. Since our proposed modules are lightweight, cascade learning does not lead to much computation cost during the inference while contributes to a significant gain on final results.

Network Architecture: Fig. 2 illustrates the whole network architecture, which bases on the state-of-the-art semantic segmentation model DeeplabV3+ [8]. Here we utilize dilated ResNet as backbone [21, 68] only for illustration purpose. The output stride of backbone is 8 in our experiment unless otherwise specified. Our designed cascade decoder is inserted after the ASPP module [8], the output feature of ASPP module is served as the input feature F_{in} in the first stage. Our method can be easily added to other methods [45, 73, 15] which can be found in the experiment part.

Loss function Design: There are three different prediction results at each cascade stage, namely F_b , F_r , F_m , which are predictions of edge part, residual part and merge part, respectively. We define a joint loss function to supervise

them simultaneously shown in Equ. 8.

$$L_{joint} = \lambda_1 L_{residual}(F_r, G_r) + \lambda_2 L_{edge}(F_b, G_e) + \lambda_3 L_{merge}(F_m, G_m) \quad (8)$$

G_m represents the original ground truth, the ground truth of edge part G_e generated from G_m is a binary edge mask with thickness 8. When generating the ground truth of residual part G_r the corresponding position of the positive pixel of G_e in G_r is marked as ignore and the other pixels of G_r are the same as G_m . λ_1 , λ_2 and λ_3 are hyper-parameters which balance the importance between $L_{residual}$, L_{edge} and L_{merge} and we set $\lambda_1 = 1$, $\lambda_2 = 3$, $\lambda_3 = 1$ in our experiments. L_{merge} and $L_{residual}$ are standard Cross-Entropy(CE) Loss. L_{edge} is Dice Loss [48]. Since our network is a cascade paradigm, the final loss function is an addition of each stage, formulated as $L = \sum_{n=1}^N L_{joint}^n$, where N represents the number of cascade layer.

4. Experiment

In this section, we verify our method on three recent proposed glass-like object segmentation datasets including Trans10K [61], MSD [65], and GDD [47]. We further prove the generality of our method on Three general segmentation datasets, including Cityscapes [12], BDD [67], and COCO Stuff [4].

4.1. Datasets and evaluation metrics

Datasets: **(a) Trans10k** dataset contains 10,428 images with two categories of transparent objects, including things and stuff. For this dataset, 5000, 1000, and 4428 images are used for train, validation, and test. **(b) GDD** is another large-scale glass object segmentation dataset covering diverse daily-life scenes (such as office, street). For dataset split, 2,980 images are randomly selected for training and the remaining 936 images are used for testing. **(c) MSD** is a recent large-scale mirror dataset containing mirrors and annotated mirror masks. For dataset split, 3,063 images are used for training while 955 images are used for testing. We use the Trans10k for ablation studies and analyses and also report results on the GDD and MSD.

Evaluation metrics: Following previous work [61, 47, 65], for the Trans10k dataset, we adopt four metrics for quantitatively evaluating the model performance unless otherwise specified. Specifically, we use the (mean) intersection over union (IoU/mIoU) and pixel accuracy (ACC) metrics from the semantic segmentation field. Mean absolute error (mAE) from the salient object detection field is also used. Finally, we use the balance error rate(BER/mBER), which considers the unbalanced areas of transparent (mirror) and non-transparent (non-mirror) regions. F-measure is also used to evaluate the model performance of GDD and MSD datasets [47, 65].

4.2. Experiment on Transparent10k

Overview: We firstly perform ablation studies on the validation set. Then visualization analysis is given to show the accurate segmentation results. Finally, we compare with the state-of-the-art methods on the test set.

Trans10k implementation detail: We adopt the same training setting as the original Trans10k [61] for fair comparison. The input images are resized to the resolution of 512×512. We use the pre-trained ResNet50 as the feature extraction network. We use 8 GPUs for all experiments and batch size is set to 4 per GPU. The learning rate is initialized to 0.01 and decayed by the poly strategy with the power of 0.9 for 16 epochs. We report mIoU, mBER, mAE in ablation study and also report ACC when comparing with the state-of-the-art methods on test set.

Ablation on Each Components: We first verify the effectiveness of each module using DeeplabV3+ [8] as the baseline in Tab. 1(a). After using our proposed RDM, there exists a significant gain over the baseline by 3.8% mIoU, 2.1 in mBER and 0.021 in mAE. These results indicate the importance of precise boundaries generation for glass object segmentation. After appending more modules in the cascade framework, the performance further gains 0.9% mIoU. Finally, based on the precise boundary, applying our proposed PGM, our method gain 0.6% mIoU on the strong baseline. Although PGM does not provide as much numerical improvement as RDM because of the small number of pixels at the boundaries, it does provide a significant visual improvement, as shown in Fig. 4(c).

Ablation on Loss function design: Then we explore the effect of loss function choice by fixing each component where the number of sample points is set to 96 in PGM, and the cascade number is set to 3. Results are shown in Tab. 1(b), after using L_{edge} , we found 1.1% mIoU gain, with an additional $L_{residual}$, we found another 1.0% mIoU gain which indicates that dual supervision is conducive to sharpen edge generation and improve the final prediction. Compared to using binary Cross-Entropy(bce) loss as L_{edge} , using dice loss [48] leads to 0.3% mIoU gain since dice loss can better handle the imbalance problems for foreground objects.

Ablation on RDM: We give detailed ablation studies on each component in RDM by removing it from the complete RDM in Tab. 1(c) where we set the cascade number to 1. Removing F_{low} or F_{high} in the first step or the second step of RDM will result in mIoU degradation of 0.4% and 0.8%, respectively. Removing both of them results in mIoU degradation of 1.0%. After removing the subtraction operation and residual learning, there is a clear drop on all metrics indicating the importance of boundary sharpening.

Ablation on boundary refinement: We present a detailed comparison on boundary using F1-score [55] with four different thresholds in Tab. 1(d). For different thresholds, results obtain significant gains after using RDM. The gain be-

Baseline	+RDM	+cascade	+pointGCN	mIoU \uparrow	mBER \downarrow	mAE \downarrow
Deeplabv3+	-	-	-	85.4	6.73	0.075
	✓	-	-	89.2	4.63	0.054
	✓	✓	-	90.1	4.15	0.049
	✓	✓	✓	90.7	3.97	0.047

(a) Effect of each component.

Settings	mIoU \uparrow	mBER \downarrow	mAE \downarrow
All operators	89.2	4.63	0.054
w/o F_{low}	88.8	4.92	0.059
w/o F_{high}	88.4	5.01	0.058
w/o Both	88.2	4.98	0.058
w/o residual learning	86.4	6.17	0.070

(c) Effect of each component in RDM.

Method	mIoU \uparrow	F1(12px) \uparrow	F1(9px) \uparrow	F1(5px) \uparrow	F1(3px) \uparrow
baseline	85.4	77.6	73.5	66.6	56.7
+RDM	89.2	84.7	81.6	77.6	68.5
+RDM & PGM	89.5	85.8	83.1	79.2	73.3

(d) Effectiveness on boundary refinement.

L_{merge}	$L_{edge-bce}$	$L_{edge-dice}$	$L_{residual}$	mIoU \uparrow	mBER \downarrow	mAE \downarrow
✓	-	-	-	88.3	5.02	0.060
✓	✓	-	-	89.4	4.48	0.053
✓	✓	-	✓	90.4	4.12	0.049
✓	-	✓	✓	90.7	3.97	0.047

(b) Effect of loss function design.

Network	mIoU \uparrow	mBER \downarrow	mAE \downarrow
FCN	83.2	7.94	0.094
+our modules	87.9	5.04	0.062
PSPNet [73]	83.5	8.34	0.089
+our modules	88.6	4.93	0.058
DANet [15]	84.1	7.03	0.084
+our modules	87.8	5.14	0.062

(e) Application on Other Architectures.

Table 1: Ablation studies. We first verify the effect of each module and loss function in (a) and (b) in terms of mIoU, mBER and mAE. Then we give a detailed component analysis in RDM in (c), and use boundary metrics to verify each module’s effect in (d). Finally, verify the various architectures in (e) to show the generality of our proposed modules. All the results are reported on the validation set of Trans10k. Best view it on screen and zoom in.

Method	mIoU \uparrow	mBER \downarrow	mAE \downarrow
Deeplabv3+(baseline)	85.4	6.73	0.075
PointRend [30]	88.2	4.86	0.060
Translab [61]	88.9	4.91	0.056
GSCNN [55]	88.2	5.10	0.059
EBLNet	89.5	4.54	0.051

Table 2: Comparison results with related methods on Trans10k validation set. All the models are trained in the same setting and tested with a single scale inference on the Trans10k validation set.

comes more significant when the neighbor pixels decrease (from 12 pixels to 3 pixels). That indicates that our method can generate a sharp and precise boundary. The improvement of mIoU also proves our motivation that better boundary prediction is beneficial to produce better segmentation results. After using PGM, there are more gains in all the metrics in this strong baseline.

Application on more segmentation methods: In addition to DeeplabV3+, we carry on experiments on various other network architectures including, FCN [45], PSPNet [73] and DANet [15]. Our modules are appended at the end of the network head, and are trained with the same setting as DeeplabV3+. As shown in Tab. 1(e), our modules improve those methods by a large margin, which proves the generality of our modules.

Comparison with related methods: We select three representative works on segmentation boundary learning [55, 30, 61]. We use DeeplabV3+ with ResNet50 backbone as the baseline model for comparison. As shown in Tab. 2, our method achieves better results than those works on three metrics with **only one** RDM and **one** PGM involved.

Comparison with the state-of-the-arts: Following [61], we report mIoU, Acc, mAE, mBER on trans10k test set. As shown in Tab. 3, our method achieves the state-of-the-art results on four metrics with output stride 16 for fair comparison with Translab [61]. After changing the output stride

Method	mIoU \uparrow	Acc \uparrow	mAE \downarrow	mBER \downarrow
Deeplabv3+(MobileNetv2) [8]	75.27	80.92	0.130	12.49
HRNet [57]	74.56	75.82	0.134	13.52
BiSeNet [66]	73.93	77.92	0.140	13.96
DenseAspp [64]	78.11	81.22	0.114	12.19
Deeplabv3+(ResNet50) [8]	84.54	89.54	0.081	7.78
FCN [45]	79.67	83.79	0.108	10.33
RefineNet [39]	66.03	57.97	0.180	22.22
Deeplabv3+(Xception65) [8]	84.26	89.18	0.082	8.00
PSPNet [73]	82.38	86.25	0.093	9.72
Translab [61]	87.63	92.69	0.063	5.46
EBLNet(OS16)	89.58	93.95	0.052	4.60
EBLNet(OS8)	90.28	94.71	0.048	4.14

Table 3: Comparison to state-of-the-art on Trans10k test set. All methods are trained on Trans10k training set under the same setting and all models use single scale inference. OS means the output stride in the backbone.

into 8 in the backbone, our method obtains a better result.

4.3. Experiment on GDD and MSD

Experiment on GDD: We adopt the same setting as the original paper [47] for fair comparison where the input images are resized into 416×416 and are augmented by horizontally random flipping. The total training epoch is 200, and the learning rate is initialized to 0.003 and decayed by the poly strategy with the power of 0.9. We also give the different backbone results for better comparison. As shown in Tab. 4, our method achieves the state-of-the-art result on this dataset on five different metrics without using CRF post-processing.

Experiment on MSD: Following the setting in MirrorNet [65], input images are resized to a resolution of 384×384 and are augmented by horizontally random flipping. The learning rate is initialized to 0.002 and decayed by the poly strategy with the power of 0.9 for 160 epochs. As shown in Tab. 5, our method achieves state-of-the-art results for four different metrics.

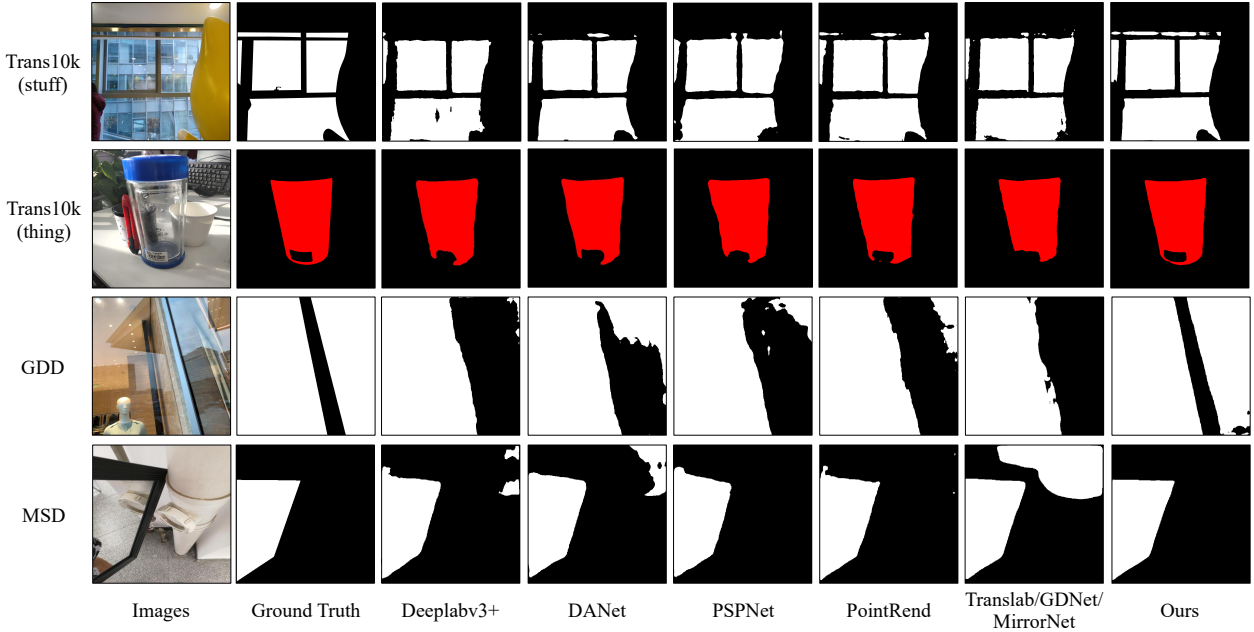


Figure 5: Visualization and comparison results on Three glass-like object segmentation datasets. The 1st and 2nd row of the 7th column are results of Translab [61], the 3rd row of the 7th column is a result of GDNet [47], the 4th row of the 7th column is a result of Mirrornet [65]. Compared with other methods, our method has much better results.

Method	IoU↑	Acc↑	F_β ↑	mAE↓	BER↓
PSPNet [73]	84.06	0.916	0.906	0.084	8.79
DenseASPP [64]	83.68	0.919	0.911	0.081	8.66
DANet [15]	84.15	0.911	0.901	0.089	8.96
CCnet [25]	84.29	0.915	0.904	0.085	8.63
PointRend [31] (Deeplabv3+)	86.51	0.933	0.928	0.067	6.50
DSS [23]	80.24	0.898	0.890	0.123	9.73
PiCANet [43]	83.73	0.916	0.909	0.093	8.26
BASNet [51]	82.88	0.907	0.896	0.094	8.70
EGNet [74]	85.04	0.920	0.916	0.083	7.43
DSC [24]	83.56	0.914	0.911	0.090	7.97
BDRAR [78] †	80.01	0.902	0.908	0.098	9.87
MirrorNet [65](ResNext101) †	85.07	0.918	0.903	0.083	7.67
GDNet [47](ResNext101)	87.63	0.939	0.937	0.063	5.62
EBLNet(ResNet101)	88.16	0.941	0.939	0.059	5.58
EBLNet((ResNext101))	88.72	0.944	0.940	0.055	5.36

†CRF is used for post-processing.

Table 4: Comparison to state-of-the-art on GDD test set. All methods are trained on GDD training set under the same setting and all models use single scale inference.

Visual Results Comparison: Fig. 5 gives the some visual results on all the three datasets. Our method can obtain superior segmentation results compared with current methods and has fine-grained boundary results on mirrors or glass. More results can be found in the supplemental file.

Efficiency and Effectiveness: To further show our method’s efficiency and effectiveness on glass-like object segmentation, we compare parameters and inference time of our network with recent glass-like object segmentation networks, including GDDNet [47] and MirrorNet [65] on the

Method	CRF	IoU↑	Acc↑	F_β ↑	mAE↓	BER↓
PSPNet [73]	-	63.21	0.750	0.746	0.117	15.82
ICNet [72]	-	57.25	0.694	0.710	0.124	18.75
PointRend [31] (Deeplabv3+)	-	78.81	0.936	0.872	0.054	8.95
Mask RCNN [19]	-	63.18	0.821	0.756	0.095	14.35
DSS [23]	-	59.11	0.665	0.743	0.125	18.81
PiCANet [43]	-	71.78	0.845	0.808	0.088	10.99
RAS [9]	-	60.48	0.695	0.758	0.111	17.60
DSC [24]	-	69.71	0.816	0.812	0.087	11.77
BDRAR [78]	✓	67.43	0.821	0.792	0.093	12.41
MirrorNet(ResNeXt101) [65]	✓	78.95	0.935	0.857	0.065	6.39
EBLNet(ResNet101)	-	78.84	0.946	0.873	0.054	8.84
EBLNet(ResNext101)	-	80.33	0.951	0.883	0.049	8.63

Table 5: Comparison to state-of-the-art on MSD test set. All methods are trained on the MSD training set. All models use single-scale inference.

Method	Parameters ↓	Inference Time ↓	mIoU↑	BER↑	mAE↑
MirrorNet[65]	103.3M	37ms	81.3	8.98	0.094
GDDNet[47]	183.2M	41ms	82.6	8.42	0.088
EBLNet	46.2M	24ms	86.0	6.90	0.074

Table 6: Comparison results with related specific methods on GDD test set. The speeds are tested with 416×416 inputs. All the inference times are tested with one V100 GPU for fair comparison.

GDD test set. All models use ResNet50 as the backbone and use the same inference setting. Results are shown in Tab. 6. Our method has much fewer parameters and faster inference speed. Besides, our method also outperforms those works by a significant margin on mIoU, BER, and mAE.

Method	backbone	dataset	mIoU ↑	F1(12px) ↑	F1(9px) ↑	F1(5px) ↑	F1(3px) ↑
Deeplabv3+ [8] +PointRend [73] +ours	ResNet50	Cityscapes	77.4	78.9	77.5	73.9	62.3
	ResNet50	Cityscapes	78.3	79.5	78.5	74.3	63.6
	ResNet50	Cityscapes	79.1	81.4	80.1	76.5	67.0
Deeplabv3+ [8] +PointRend [73] +ours	ResNet50	BDD	60.8	76.4	75.2	70.6	61.5
	ResNet50	BDD	61.2	78.4	77.2	72.3	63.6
	ResNet50	BDD	63.1	80.6	79.4	75.4	66.4
Deeplabv3+ [8] +PointRend [73] +ours	ResNet50	COCO Stuff	33.6	73.3	71.8	70.6	66.7
	ResNet50	COCO Stuff	34.1	73.8	72.3	71.1	67.4
	ResNet50	COCO Stuff	34.7	74.9	72.9	71.5	67.7

Table 7: Comparison results on Cityscapes, BDD and COCO Stuff datasets with DeeplabV3+ and PointRend where X-px means X pixels along the boundaries. All the models are trained in the same setting and are tested with single-scale inference.

4.4. Generalization on More Segmentation Datasets

In this section, we prove the generality and effectiveness of our method on another three general segmentation datasets, including Cityscapes [12], BDD [67] and COCO Stuff [4]. We adopt the same training settings for fair comparison, which can be found in the supplemental file. We report both mIoU and F-score on boundary [55] with four thresholds.

Baseline and Results: We use the DeeplabV3+ as the baseline method. Results are shown in Tab. 7. For Cityscapes dataset, our method obtains 1.7% mIoU over baseline and 0.8% mIoU over PointRend. After adopting F-score as evaluation metric, our method results in a large margin in boundary accuracy. For BDD dataset, our method obtains 2.3% mIoU higher than baseline and 1.9% mIoU higher than PointRend. F-score can also demonstrate the superiority of our method on BDD dataset. For COCO stuff dataset, compared with the baseline, our method obtains 1.1% mIoU gain and 0.6% mIoU gain over PointRend. Our method also obtains performance gain over baseline and PointRend on F-score.

5. Conclusion

In this paper, we focus on solving the glass-like object segmentation problem by enhancing the boundary learning for existing segmentation methods. We propose a novel Refined Differential Module for edge prediction and an efficient edge-aware Point-wised Graph convolution network Module to model global shape representation of glass objects and guide the final prediction. We achieve the new state-of-the-art results on three recent glass-like object segmentation datasets, including Trans10k, MSD, and GDD. Further experiments on three general segmentation datasets, including Cityscapes, BDD, and COCO Stuff prove the generality and superiority of our method.

References

[1] Pablo Arbelaez, Michael Maire, Charless Fowlkes, and Jitendra Malik. Contour detection and hierarchical image seg-

mentation. *IEEE transactions on pattern analysis and machine intelligence*, 2010.

[2] Gedas Bertasius, Jianbo Shi, and Lorenzo Torresani. Semantic segmentation with boundary neural fields. In *CVPR*, 2016.

[3] Gedas Bertasius, Lorenzo Torresani, Stella X. Yu, and Jianbo Shi. Convolutional random walk networks for semantic image segmentation. In *CVPR*, 2017.

[4] Holger Caesar, Jasper Uijlings, and Vittorio Ferrari. Coco-stuff: Thing and stuff classes in context. In *CVPR*, 2018.

[5] Zhaowei Cai and Nuno Vasconcelos. Cascade r-cnn: Delving into high quality object detection. In *CVPR*, 2018.

[6] Nicolas Carion, Francisco Massa, Gabriel Synnaeve, Nicolas Usunier, Alexander Kirillov, and Sergey Zagoruyko. End-to-end object detection with transformers. In *ECCV*, 2020.

[7] Liang-Chieh Chen, George Papandreou, Florian Schroff, and Hartwig Adam. Rethinking atrous convolution for semantic image segmentation. *arXiv preprint*, 2017.

[8] Liang-Chieh Chen, Yukun Zhu, George Papandreou, Florian Schroff, and Hartwig Adam. Encoder-decoder with atrous separable convolution for semantic image segmentation. In *ECCV*, 2018.

[9] Shuhan Chen, Xiuli Tan, Ben Wang, and Xuelong Hu. Reverse attention for salient object detection. In *ECCV*, 2018.

[10] Xier Chen, Yanchao Lian, Licheng Jiao, Haoran Wang, Yan-Jie Gao, and Shi Lingling. Supervised edge attention network for accurate image instance segmentation. In *ECCV*, 2020.

[11] Tianheng Cheng, Xinggang Wang, Lichao Huang, and Wenyu Liu. Boundary-preserving mask r-cnn. In *ECCV*, 2020.

[12] Marius Cordts, Mohamed Omran, Sebastian Ramos, Timo Rehfeld, Markus Enzweiler, Rodrigo Benenson, Uwe Franke, Stefan Roth, and Bernt Schiele. The cityscapes dataset for semantic urban scene understanding. In *CVPR*, 2016.

[13] Ruoxi Deng, Chunhua Shen, Shengjun Liu, Huibing Wang, and Xinru Liu. Learning to predict crisp boundaries. In *ECCV*, 2018.

[14] Adrian N Evans and Xin U Liu. A morphological gradient approach to color edge detection. *TIP*, 2006.

[15] Jun Fu, Jing Liu, Haijie Tian, Zhiwei Fang, and Hanqing Lu. Dual attention network for scene segmentation. In *CVPR*, 2019.

[16] Shang-Hua Gao, Yong-Qiang Tan, Ming-Ming Cheng, Chengze Lu, Yunpeng Chen, and Shuicheng Yan. Highly efficient salient object detection with 100k parameters. In *ECCV*, 2020.

[17] Junjun He, Zhongying Deng, and Yu Qiao. Dynamic multi-scale filters for semantic segmentation. In *ICCV*, 2019.

[18] Junjun He, Zhongying Deng, Lei Zhou, Yali Wang, and Yu Qiao. Adaptive pyramid context network for semantic segmentation. In *CVPR*, 2019.

[19] Kaiming He, Georgia Gkioxari, Piotr Dollar, and Ross Girshick. Mask r-cnn. In *ICCV*, 2017.

[20] Kaiming He, Xiangyu Zhang, Shaoqing Ren, and Jian Sun. Delving deep into rectifiers: Surpassing human-level performance on imagenet classification. In *ICCV*, 2015.

[21] Kaiming He, Xiangyu Zhang, Shaoqing Ren, and Jian Sun. Deep residual learning for image recognition. In *CVPR*, 2016.

[22] Xuming He and Stephen Gould. An exemplar-based crf for multi-instance object segmentation. In *CVPR*, 2014.

[23] Qibin Hou, Ming-Ming Cheng, Xiaowei Hu, Ali Borji, Zhuowen Tu, and Philip Torr. Deeply supervised salient object detection with short connections. In *CVPR*, 2017.

[24] Xiaowei Hu, Lei Zhu, Chi-Wing Fu, Jing Qin, and Pheng-Ann Heng. Direction-aware spatial context features for shadow detection. In *CVPR*, 2018.

[25] Zilong Huang, Xinggang Wang, Lichao Huang, Chang Huang, Yunchao Wei, and Wenyu Liu. Ccnet: Criss-cross attention for semantic segmentation. In *ICCV*, 2019.

[26] Sergey Ioffe and Christian Szegedy. Batch normalization: Accelerating deep network training by reducing internal covariate shift. In *ICML*, 2015.

[27] Agastya Kalra, Vage Taamazyan, Supreeth Krishna Rao, Kartik Venkataraman, Ramesh Raskar, and Achuta Kadambi. Deep polarization cues for transparent object segmentation. In *CVPR*, 2020.

[28] Tsung-Wei Ke, Jyh-Jing Hwang, Ziwei Liu, and Stella X. Yu. Adaptive affinity fields for semantic segmentation. In *ECCV*, 2018.

[29] Thomas N Kipf and Max Welling. Semi-supervised classification with graph convolutional networks. In *ICLR*, 2017.

[30] Alexander Kirillov, Yuxin Wu, Kaiming He, and Ross Girshick. PointRend: Image segmentation as rendering. In *CVPR*, 2020.

[31] Alexander Kirillov, Yuxin Wu, Kaiming He, and Ross Girshick. Pointrend: Image segmentation as rendering. In *CVPR*, 2020.

[32] Iasonas Kokkinos. Pushing the boundaries of boundary detection using deep learning. *arXiv preprint arXiv:1511.07386*, 2015.

[33] Xiangtai Li, Xia Li, Li Zhang, Guangliang Cheng, Jianping Shi, Zhouchen Lin, Shaohua Tan, and Yunhai Tong. Improving semantic segmentation via decoupled body and edge supervision. In *ECCV*, 2020.

[34] Xiangtai Li, Ansheng You, Zhen Zhu, Houlong Zhao, Maoke Yang, Kuiyuan Yang, and Yunhai Tong. Semantic flow for fast and accurate scene parsing. *ECCV*, 2020.

[35] Xiangtai Li, Li Zhang, Ansheng You, Maoke Yang, Kuiyuan Yang, and Yunhai Tong. Global aggregation then local distribution in fully convolutional networks. *arXiv preprint arXiv:1909.07229*, 2019.

[36] Xia Li, Zhisheng Zhong, Jianlong Wu, Yibo Yang, Zhouchen Lin, and Hong Liu. Expectation-maximization attention networks for semantic segmentation. In *ICCV*, 2019.

[37] Yin Li and Abhinav Gupta. Beyond grids: Learning graph representations for visual recognition. *NeurIPS*, 2018.

[38] Xiaodan Liang, Zhiting Hu, Hao Zhang, Liang Lin, and Eric P Xing. Symbolic graph reasoning meets convolutions. In S. Bengio, H. Wallach, H. Larochelle, K. Grauman, N. Cesa-Bianchi, and R. Garnett, editors, *NeurIPS*, 2018.

[39] Guosheng Lin, Anton Milan, Chunhua Shen, and Ian D. Reid. Refinenet: Multi-path refinement networks for high-resolution semantic segmentation. In *CVPR*, 2017.

[40] Guosheng Lin, Chunhua Shen, Anton van den Hengel, and Ian Reid. Efficient piecewise training of deep structured models for semantic segmentation. In *CVPR*, 2016.

[41] Jiang-Jiang Liu, Qibin Hou, Ming-Ming Cheng, Jiashi Feng, and Jianmin Jiang. A simple pooling-based design for real-time salient object detection. In *CVPR*, 2019.

[42] Nian Liu and Junwei Han. Dhsnet: Deep hierarchical saliency network for salient object detection. In *CVPR*, 2016.

[43] Nian Liu, Junwei Han, and Ming Hsuan Yang. Picanet: Learning pixel-wise contextual attention for saliency detection. *CVPR*, 2017.

[44] Ziwei Liu, Xiaoxiao Li, Ping Luo, Chen-Change Loy, and Xiaoou Tang. Semantic image segmentation via deep parsing network. In *ICCV*, 2015.

[45] Jonathan Long, Evan Shelhamer, and Trevor Darrell. Fully convolutional networks for semantic segmentation. In *CVPR*, 2015.

[46] Kevis-Kokitsi Maninis, Jordi Pont-Tuset, Pablo Arbeláez, and Luc Van Gool. Convolutional oriented boundaries: From image segmentation to high-level tasks. *PAMI*, 2017.

[47] Haiyang Mei, Xin Yang, Yang Wang, Yuanyuan Liu, Shengfeng He, Qiang Zhang, Xiaopeng Wei, and Rynson W.H. Lau. Don't hit me! glass detection in real-world scenes. In *CVPR*, 2020.

[48] Fausto Milletari, Nassir Navab, and Seyed-Ahmad Ahmadi. V-net: Fully convolutional neural networks for volumetric medical image segmentation. In *3DV*. IEEE, 2016.

[49] Youwei Pang, Xiaoqi Zhao, Lihe Zhang, and Huchuan Lu. Multi-scale interactive network for salient object detection. In *CVPR*, 2020.

[50] Giuseppe Papari and Nicolai Petkov. Edge and line oriented contour detection: State of the art. *IMAGE VISION COMPUT*, 2011.

[51] Xuebin Qin, Zichen Zhang, Chenyang Huang, Chao Gao, Masood Dehghan, and Martin Jagersand. Basnet: Boundary-aware salient object detection. In *CVPR*, 2019.

[52] Jean-Francois Rivest, Pierre Soille, and Serge Beucher. Morphological gradients. *Journal of Electronic Imaging*, 1993.

[53] Wei Shen, Xinggang Wang, Yan Wang, Xiang Bai, and Zhi-jiang Zhang. Deepcontour: A deep convolutional feature learned by positive-sharing loss for contour detection. In *CVPR*, 2015.

[54] Nathan Silberman, Derek Hoiem, Pushmeet Kohli, and Rob Fergus. Indoor segmentation and support inference from rgbd images. In *ECCV*. Springer, 2012.

[55] Towaki Takikawa, David Acuna, Varun Jampani, and Sanja Fidler. Gated-scnn: Gated shape cnns for semantic segmentation. *ICCV*, 2019.

[56] Ashish Vaswani, Noam Shazeer, Niki Parmar, Jakob Uszkoreit, Llion Jones, Aidan N Gomez, Łukasz Kaiser, and Illia Polosukhin. Attention is all you need. In *NeurIPS*, 2017.

[57] Jingdong Wang, Ke Sun, Tianheng Cheng, Borui Jiang, Chaorui Deng, Yang Zhao, Dong Liu, Yadong Mu, Mingkui Tan, Xinggang Wang, et al. Deep high-resolution representation learning for visual recognition. *PAMI*, 2020.

[58] Xiaolong Wang, Ross Girshick, Abhinav Gupta, and Kaiming He. Non-local neural networks. In *CVPR*, 2018.

[59] Svante Wold, Kim Esbensen, and Paul Geladi. Principal component analysis. *Chemom. Intell. Lab. Syst.*, 1987.

[60] Zhe Wu, Li Su, and Qingming Huang. Cascaded partial decoder for fast and accurate salient object detection. In *CVPR*, 2019.

[61] Enze Xie, Wenjia Wang, Wenhai Wang, Mingyu Ding, Chunhua Shen, and Ping Luo. Segmenting transparent objects in the wild. *ECCV*, 2020.

[62] Enze Xie, Wenjia Wang, Wenhai Wang, Peize Sun, Hang Xu, Ding Liang, and Ping Luo. Segmenting transparent object in the wild with transformer. *arXiv preprint arXiv:2101.08461*, 2021.

[63] Saining Xie and Zhuowen Tu. Holistically-nested edge detection. In *ICCV*, 2015.

[64] Maoke Yang, Kun Yu, Chi Zhang, Zhiwei Li, and Kuiyuan Yang. Denseaspp for semantic segmentation in street scenes. In *CVPR*, 2018.

[65] Xin Yang, Haiyang Mei, Ke Xu, Xiaopeng Wei, Baocai Yin, and Rynson WH Lau. Where is my mirror? In *ICCV*, 2019.

[66] Changqian Yu, Jingbo Wang, Chao Peng, Changxin Gao, Gang Yu, and Nong Sang. Bisenet: Bilateral segmentation network for real-time semantic segmentation. In *ECCV*, 2018.

[67] Fisher Yu, Haofeng Chen, Xin Wang, Wenqi Xian, Yingying Chen, Fangchen Liu, Vashisht Madhavan, and Trevor Darrell. Bdd100k: A diverse driving dataset for heterogeneous multitask learning. In *CVPR*, 2020.

[68] Fisher Yu and Vladlen Koltun. Multi-scale context aggregation by dilated convolutions. *ICLR*, 2016.

[69] Zhiding Yu, Chen Feng, Ming-Yu Liu, and Srikumar Ramalingam. Casenet: Deep category-aware semantic edge detection. In *CVPR*, 2017.

[70] Lu Zhang, Ju Dai, Huchuan Lu, You He, and Gang Wang. A bi-directional message passing model for salient object detection. In *CVPR*, 2018.

[71] Pingping Zhang, Dong Wang, Huchuan Lu, Hongyu Wang, and Xiang Ruan. Amulet: Aggregating multi-level convolutional features for salient object detection. *CVPR*, 2017.

[72] Hengshuang Zhao, Xiaojuan Qi, Xiaoyong Shen, Jianping Shi, and Jiaya Jia. Icnet for real-time semantic segmentation on high-resolution images. In *ECCV*, 2018.

[73] Hengshuang Zhao, Jianping Shi, Xiaojuan Qi, Xiaogang Wang, and Jiaya Jia. Pyramid scene parsing network. In *CVPR*, 2017.

[74] Jia-Xing Zhao, Jiang-Jiang Liu, Deng-Ping Fan, Yang Cao, Jufeng Yang, and Ming-Ming Cheng. Egnet: Edge guidance network for salient object detection. In *ICCV*, 2019.

[75] Xiaoqi Zhao, Youwei Pang, Lihe Zhang, Huchuan Lu, and Lei Zhang. Suppress and balance: A simple gated network for salient object detection. In *ECCV*, 2020.

[76] Shuai Zheng, Sadeep Jayasumana, Bernardino Romera-Paredes, Vibhav Vineet, Zhizhong Su, Dalong Du, Chang Huang, and Philip H. S. Torr. Conditional random fields as recurrent neural networks. In *ICCV*, 2015.

[77] Bolei Zhou, Hang Zhao, Xavier Puig, Tete Xiao, Sanja Fidler, Adela Barriuso, and Antonio Torralba. Semantic understanding of scenes through the ade20k dataset. *IJCV*.

[78] Lei Zhu, Zijun Deng, Xiaowei Hu, Chi-Wing Fu, Xuemiao Xu, Jing Qin, and Pheng-Ann Heng. Bidirectional feature pyramid network with recurrent attention residual modules for shadow detection. In *ECCV*, 2018.

[79] Zhen Zhu, Mengde Xu, Song Bai, Tengteng Huang, and Xiang Bai. Asymmetric non-local neural networks for semantic segmentation. In *ICCV*, 2019.